Atmos. Meas. Tech. Discuss., 6, 3249–3277, 2013
www.atmos-meas-tech-discuss.net/6/3249/2013/
doi:10.5194/amtd-6-3249-2013

Atmospheric Measurement Techniques Discussions

One-year analysis of rain and rain erosivity in a tropical volcanic island from UHF wind profiler measurements

A. Réchou[1], M. Plu[1], B. Campistron[2], and R. Decoupes[3]

[1]Laboratoire de l'Atmosphère et des Cyclones, UMR8105, Université de la Réunion, Bâtiment S4B, 15, avenue René Cassin – CS 92003, 97744 Saint-Denis Cedex 9, Ile de La Réunion, France
[2]Laboratoire d'Aérologie, OMP – UMR5560, Observatoire Midi Pyrénées, Toulouse, France
[3]Observatoire des Sciences de l'Univers à la Réunion, UMS3365, Université de la Réunion, Bâtiment S4B, 115, avenue René Cassin – CS 92003, 97744 Saint-Denis Cedex 9, Ile de La Réunion, France

Received: 14 March 2013 – Accepted: 24 March 2013 – Published: 4 April 2013

Correspondence to: A. Réchou (arechou@univ-reunion.fr)

Published by Copernicus Publications on behalf of the European Geosciences Union.

Abstract

La Réunion is a volcanic island in a tropical zone, which soil undergoes intense erosion. The possible contribution of rainfall to erosion is analyzed and quantified using one year of UHF radar profiler data located at sea level. Measurements of reflectivity, vertical and horizontal wind allow, with suitable assumptions, to determine raindrop vertical and horizontal energy fluxes, which are both essential parameters for erosion.

After calibration of radar rain rates, one-year statistics between May 2009 to April 2010 allow to identify differences in rain vertical profiles depending on the season. During the cool dry season, the mean rain rate is less than 2.5 mm h^{-1} as high as 1.25 km and it decreases at higher altitudes due to the trade winds inversion. During the warm moist season, the mean rain rate is nearly uniform from ground up to 4 km, around 5 mm h^{-1}. The dynamical and microphysical properties of rainfall events are investigated on three cases that are representative of meteorological events in La Réunion: summer deep convection, a cold front and a winter depression embedded in trade winds. For intense rainfall events, the rain rate deduced from the gamma function is in agreement with the rain rate deduced from the mere Marshall Palmer exponential relationship. For less intense events, the gamma function is necessary to represent rain distribution. The deep-convection event is associated to strong reflectivity reaching as high as 10 km, and strong negative vertical velocity. Wind shear is responsible for a deficiency of radar rain detection at the lower levels. During a cold front event, strong reflectivities reach the trade wind inversion (around 4 km high). The trade wind depression generates moderate rain only as high as 2 km. For all the altitudes, the horizontal kinetic energy fluxes are one order of magnitude stronger that than the vertical kinetic energy fluxes. A simple relationship between the reflectivity factor and vertical kinetic energy fluxes is found for each case study.

AMTD
6, 3249–3277, 2013

1 Introduction

Soil erosion generally impacts living activities, vegetation, terrain use and landscape modeling. Since la Réunion Island is a tropical island, rainfall and soil erosion are particularly intense. Rainfall events and their possible impact on erosion need to be characterized. In the tropics, most of the studies are about the Northern Hemisphere. In Taiwan (from 120 to 122° E, and from 22 to 25° N), the characteristics of rainfall distributions were analyzed during the Taiwan Area Mesoscale Experiment (TAMEX) (Johnson and Bresch, 1991) using soundings, surface precipitation, and radar data. They found two primary characteristics of precipitation. Major rainfall events are linked to the passage of midlatitude disturbances and they consist in both deep convective (prefrontal or frontal) and stratiform (postfrontal in association with overrunning and orographic lifting) components. Seasonal changes of prevailing wind and atmospheric stability allow Chen and Chen (2003) to separate the year into five separate regimes (winter, spring, mei-yu, summer and automn) using 38 yr rainfall data (1961–1998) from 25 conventional stations and 5 yr hourly rainfall data (1994–1998) from 249 Automatic Rainfall and Meteorological Telemetry System (ARMTS) stations (Chen et al., 1999). In Hawai (19 to 22° N, 154 to 160° W) Islands, Sanderson (1993) found that trade winds occur for 85 to 95 % of the time in summer and for 50 to 80 % of the time in winter. When trade winds fail, humidity increases and the rainfall distribution changes (Schroeder, 1993). In the Southern Hemisphere, with radiosonde data, Baldy et al. (1996) decomposed a year into two seasons, while Taupin et al. (1999) considered four seasons. In the first classification, winter is associated to an intense Hadley cell and strong trade winds, whereas summer shows deep convection and strong humidity transport. In the second classification, summer or rainy season is from December to February, when the deep convection is frequent (the ITCZ is close to La Réunion), relative humidity reaches high values and trade winds are rare. The winter season is from June to August, when the trade winds are the strongest, relative humidity is the lowest. The subtropical upper level jet stream is close to La Réunion Island (Hastenrath, 1991). March to May, and

AMTD
6, 3249–3277, 2013

September to November are two interseasons, which characteristics resemble the ones of each preceding season. Robert (1986), using raingauges in Réunion Island defined 5 types of rain: trade-winds rain, rain from tropical disturbances, rain from disturbances from the south from mid-latitude origine, rain from particular rain clouds regimes and rain from weak circulations.

Even with the development of sophisticated high-resolution mesoscale models, there is still a need for in-situ precipitation data. The ability of wind profilers (UHF or VHF) to estimate raindrop size distribution (DSD) has been demonstrated by several investigators using various techniques (Wakasugi et al., 1986; Rajopadhyaya and al., 1993). Also, Gossard (1988, 1990), used a UHF profiler for retrieving DSD in light rain. Williams (2002) showed that it is possible to retrieve DSD from a UHF profiler even during moderate to heavy rain using the Sans Air Motion (SAM) model. The precipitation spectrum is used to estimate the ambient air motion spectral width and the DSD. In comparing their data with two surface disdrometers, they found a good agreement only in heavy rain for diameter of the drop greater than 1.5 mm. Because of this difficulty to resolve small drops, Rajopadhyaya et al. (1999) revealed that such technique often overestimates the median volume diameter. Using a two frequency method, Cifelli et al. (2000) and Schafer et al. (2002) showed a good agreement with the data for every rain rates. Murata et al. (2002) examined the relationship between wind and precipitation with UHF radar, GPS Rawinsondes and Surface Meteorological Instruments at Kototabang, West Sumatera during September–October 1998.

Different theoretical probability density functions have been proposed to simulate DSD: the exponential function (Marshall and Palmer, 1948), Gaussian function (Maguire and Avery, 1994), lognormal distribution (Feingold and Levin, 1987), and the gamma function. The latter has been the most widely used to describe a variety of DSD (Kozu and Nakamur, 1991; Su and Chu, 2007), since it improves the accuracy of the rate precipitation (Ulbrich and Atlas, 1998). It is defined as $N(D) = N_o D^{\mu} e^{-\Lambda D}$ where $N(D)$ (Eq. 1) is the DSD ($m^{-3} mm^{-1}$), D the diameter (mm), N_o, the number density parameter ($m^{-3} mm^{-1-\mu}$), Λ is the slope parameter (mm^{-1}), and μ is a dimensionless

AMTD
6, 3249–3277, 2013

shape parameter. The three parameters of gamma function (N_o, Λ and μ) are not independent one to each other.

Chu and Su (2008) measured DSD from seven different independent precipitation events using a disdrometer. They determined an empirical μ–Λ relation, using a best fitting quadratic polynomial to observed data, that is slightly different from those by others scientists (Zhang et al., 2003; Brandes et al., 2004).

Rainfall properties and intensity may be analyzed in the watershed of "La Rivière des Pluies" in La Réunion using raingauges and a UHF radar located at the exit of the watershed at sea level. A raingauge is collocated with the radar. Radar-derived precipitation and winds are obtained at all heights from 800 m up to 4000 m (lower mode and higher for the upper mode), higher than the upper height of the watershed (3000 m). Such instrumental setup allows to perform a calibration of radar data and to investigate the microphysical and dynamical characteristics of rainfall over the watershed.

The article is organized as follows. First, we give a general presentation including descriptions of the geographical and climatic characteristics of La Réunion island and descriptions of the radar. Then, a one-year statistical analysis is presented from May 2009 to April 2010. After a calibration of the radar data, the rainfall rates obtained by the radar at 800 m and those obtained by a pluviometer located beside the radar will be compared. The mean precipitation in the rain and dry season will be analyzed. The analysis of three cases studies will allow to describe the rainfall event properties and the relationship between the rain rate obtained by Marshall Palmer function and gamma function. Finally, a comparison of vertical and horizontal kinetic energy fluxes (VKF, HKE resp.) will be done using the UHF radar, and a relationship between the reflectivity factor Z and vertical kinetic energy fluxes is analyzed for each case study.

AMTD
6, 3249–3277, 2013

2 General presentation

2.1 La Réunion Island

La Réunion Island emerges from sea level as two volcanic summits from the same hot spot (Courtillot et al., 1986), which explains its roughly circular shape of 60 km mean diameter and its peak at 3000 m altitude. Intense erosion due to the fragile volcanic soil and frequent strong precipitation have been responsible for a very broken relief (Fig. 1). The planeze, regularly inclined towards the sea, overhangs sub-vertical ramparts of kilometric size which borders circuses.

Due to its latitude, La Réunion Island (21° S, 55° E) is influenced by tropical and sub-tropical climates. Precipitation regimes may be divided into two main seasons. From November to April, the warm moist summer season is associated to deep convection, sometimes in relation with tropical cyclones. During this season, the most intense precipitation events happen, sometimes reaching world records (Quetelard et al., 2009). During the cool dry season (from May to October), La Réunion Island is mainly influenced by easterly trade winds. Cloud formation over the island follows a diurnal cycle and vertical cloud extension is restricted by trade wind inversion around altitude 4 km. Orographic forcing is responsible for stronger precipitation on the east leeward coast (Fig. 2). During winter, fronts originating from the mid-latitudes may reach La Réunion and generate intense precipitation events.

Generally, there are more precipitations in the upper levels than close to the littoral (Fig. 2). The maxima of precipitation are located between 1000 and 2000 m altitude. The location of the radar (Gillot) corresponds to an intermediate zone with 1 m yr^{-1} of precipitation. Saint Denis is located between the dry western zone and the eastern rainy zone (Fig. 2).

AMTD
6, 3249–3277, 2013

2.2 Presentation of the radar and methodology

The UHF profiler is a Degreane Horizon PCL1300 working with a 1290 MHz transmitted frequency at, a 3.5 kW peak-power (Campistron and Réchou, 2012). It provides during a 4 min cycle, in clear air and raining conditions, vertical profiles of reflectivity, the three components of the wind, Doppler spectral width and skewness. In order to get the three components of the wind, the profiler uses alternatively five beams, one vertical and four oblique, with a one-way half-power aperture of 8.5° (Fig. 3). The oblique beams, with an off-zenith angle of 13°, are disposed every 90° in azimuth. Vertical profiles of the radial velocity, reflectivity, and spectral width are obtained from 75 m up to a height of about 4 km, with a 75 m vertical resolution and a 5 min temporal resolution. The cycle is composed of a low (up to 4 km) and high mode (up to 10 km in some conditions) data collection. Pulse length, lower gate height, inter-gate range and the recorded vertical coverage are for the low-mode of 300 m, 82 m, 72 m, 5.6 km, and for the high-mode of 750 m, 139 m, 143 m, 10.1 km, respectively. The selection of the relevant peak in the Doppler spectra is made with a 15 min duration consensus technique based on median filter, thresholds, vertical and time continuity tests. A particular care is taken to the detection and correction of bimodal peaks resulting for instance from the concatenation of atmospheric and ground clutter echoes.

The methodology defined by Campistron and Réchou (2012) uses the set of Eqs. (1)–(9). First we assume that, on the average, the raindrop size distribution $N(D)$, where D is the diameter, follows a gamma function (Eq. 1) (Ulbrich, 1983). Equations (2) and (3) give the raindrop fall speed in still air taking into account the change of density with height (Atlas et al., 1973; Foote and du Toit, 1969). The quadratic form 4 relating μ to Λ reduces Eq. (1) to a two-parameter problem (Chu and Su, 2008). $< W_f >$ and $< Z >$, the mean vertical velocity and reflectivity factor respectively, are quantities measured by the profiler at the resolution of the pulse volume. Equations (5) and (6) are deduced from Eqs. (1) and (2) after integration over the diameter interval supposed

AMTD
6, 3249–3277, 2013

to extend from 0 to infinity. With the same procedure the expression of the precipitation rate R is obtained in Eq. (7).

$$N(D) = N_o D^{\mu} e^{-\Lambda D} \quad (1)$$

$$W_f(D) = \alpha_1 - \alpha_2 e^{-\alpha 3D} \quad (2)$$

$$\alpha_1 = 9.65(\rho_0/\rho)^{0.4} \quad \alpha_2 = 10.3(\rho_0/\rho)^{0.4} \quad \alpha_3 = 600 \quad (3)$$

$$\Lambda = 50.0\mu^2 + 1200.0\mu + 3390.0 \quad (4)$$

$$< W_f >= \alpha_1 - \alpha_2(1 + \alpha_3/\Lambda)^{-(\mu+7)} \quad (5)$$

$$< Z >= N_o \Gamma(\mu + 7)\Lambda^{-(\mu+7)} \quad (6)$$

$$R = N_o \Gamma(\mu + 4)\pi 6^{-1}(\alpha_1 \Lambda^{-(\mu+4)} - \alpha_2(\Lambda + \alpha_3)^{-(\mu+4)}) \quad (7)$$

$$HKEF = \rho_w V^2 R/2 \quad (8)$$

$$VKEF = \rho_w N_o \Gamma(\mu + 4)\pi 12^{-1}\left[\alpha_1^3 \Lambda^{-(\mu+4)} - \alpha_2^3(\Lambda + 3\alpha_3)^{-(\mu+4)} + 3\alpha_1\alpha_2^2(\Lambda + 2\alpha_3)^{-(\mu+4)} - 3\alpha_2\alpha_1^2(\Lambda + \alpha_3)^{-(\mu+4)}\right] \quad (9)$$

ρ and ρ_w are air and water density, respectively. Γ is the gamma function. mksa units are used.

The rain kinetic energy flux crossing an horizontal surface of unit area during a unit of time is decomposed here into a vertical kinetic energy flux VKEF function of drop vertical velocity W_f (Eq. 9), and a horizontal kinetic energy flux HKEF related to the raindrop entrainment by the wind velocity V (Eq. 8). Introducing expression (4) of Λ in Eq. (5) allows to derive the value of μ from the profiler measurement of $< W_f >$. With this value and Eq. (4), Λ is obtained, and consequently N_o from Eq. (6) using the profiler measurement of $< Z >$. Then we have all the material to get the value of R, HKEF and VKEF from their respective retrieval Eqs. (7)–(9). To get rain integrated parameters it is assumed that air vertical velocity is negligible compared to raindrop fallspeed. There is no easy mean to insure with only profiler information that this assumption is fulfilled. This weakness of the methodology is partly attenuated by a spectral average made

AMTD
6, 3249–3277, 2013

here over 3 radar cycles (∼ 15 min). On the other hand, only signal with vertical velocity smaller than $-2\,\mathrm{ms}^{-1}$ and larger than $-9\,\mathrm{ms}^{-1}$, reflectivity factor larger than 5 dBZ, and normalized skewness smaller than −0.1 are considered as rainechoes and retained. The threshold on skewness is very efficient to remove snow echoes.

2.3 Radar calibration

Radar calibration is an essential step in data processing. The calibration is based on the comparison between rain rate measured by the profiler and raingauge at the ground. The height of the radar data is taken as low at possible considering signal saturation, receiver linearity, and ground clutter. Then, the best level is chosen around 600 m. A period of long lasting stratiform precipitation was chosen, because it avoids strong vertical air velocities and ensures that high relative humidity minimizes rain modification during its fall. The radar constant was modified until the best agreement was found between raingauge and radar measurements. Figure 4 shows an example of comparison between the rain rate deduced from radar data and raingauge during the 9–10 March event (stratiform and convective precipitation reaching $40\,\mathrm{m\,s}^{-1}$). The time series of the comparison show a good correspondence between both instruments. The profiler underestimates the rain rate by about 10 %.

The radar time series has 15 % less data than the raingauge times series. This loss of radar data might be explained by the effect of the rejection tests on echoes coming from region with substantial air vertical velocity.

3 Analysis of the data

3.1 Statistical analysis

Between May 2009 to April 2010, there were 89 rainy days. By a comparison with raingauge and radar at 800 m (Fig. 5) precipitation rates at 800 m are stronger than at the

AMTD
6, 3249–3277, 2013

ground, which means that there is evaporation between 800 m and the ground. Moreover, strong horizontal winds due to the trade winds in dry season can also propagate the rain. On the contrary, during some of the most intense precipitating events, there is less rain detected by the radar at 800 m than by the rain gauge. This may be explained if such rainfall events are highly spatially inhomogeneous and horizontal wind may induce a difference between 800 m and the ground. The high precipitation rates in June may be explained by the passage of fronts (number of days and rainrate).

The comparison between the duration of the rain and the rainrate done at 800 m (Fig. 5b) does not show a clear correlation. But the longest periods of rain (between 6 and 8 h) occur during the wet season and in winter time in association with the passage of fronts. However, not all intense precipitation events are associated to long duration of rain.

The mean and standard deviation of rain rates during the dry (April to October 2009 and April 2010) and moist (November 2009 to March 2010) seasons reveal typical differences (Fig. 6). These seasonal statistics are built from the samples of non-zero hourly rain rates. At every altitude, precipitation observed during the rainy season is stronger than during the dry season. During the moist season, rain rates are nearly uniform from the ground up to 4 km. This is consistent with deep-convection development. During the 2009–2010 wet season, Réunion island was concerned by some tropical depressions, although it was not directly hit by a severe tropical cyclone. During the dry season, the mean rain rate reaches a maximum at 1.2 km high, and vanishes at higher altitudes. The humidity condensates maximally around 1.5 km and the inversion of the trade winds around 3 km prohibits the vertical development of clouds.

For both seasons, standard deviations are much higher than mean values, which reveals strong variability of precipitation patterns. During the dry season, the standard deviation profile is roughly proportional to the mean, which suggests that the shape of rainfall vertical profiles may not change much from one event to another: trade-wind inversion imposes a strong constraint on the vertical profiles. During the moist season, two maxima of deviation are reached: one around 1.5 km and the other around

AMTD
6, 3249–3277, 2013

2.5 km. Some events may be limited by trade-wind inversion at 3 km-altitude (similarly to dry-season events) and some may be associated to deep-convection, or depression, without trade-wind inversion. This may explain the variability of rainfall as a function of altitude during the moist season.

3.2 Analysis of three cases study among the three different periods

3.2.1 Description of the different case studies

Three different cases have been chosen in order to analyse how efficient is the UHF radar rain estimation depending on the meteorological situation. The rainy days of 2 February 2010, the 25 June and 19 August will be studied (Fig. 7) to represent different precipitation patterns. Figure 8 presents the time height sections of reflectivity factor, vertical velocity and wind velocity for these three days.

The 2 February (Fig. 8a1), reflectivities vary between the strong values 37 and 43 dBZ from 14:00 to 16:00 UTC at nearly all the altitudes of the radar range. From 16:15 to 17:30 UTC, the reflectivity vanishes, before increasing again after 17:30 UTC. Strong reflectivities are associated to strong downward vertical velocities (less than $-5\,m\,s^{-1}$) (Fig. 8a2). On that day, wind shear is also intense (Fig. 8a3): the intensity of the wind is less than $6\,m\,s^{-1}$ in the low levels and reaches $20\,m\,s^{-1}$ between above 2000 m. Such a vertical rain structure is characteristic of deep-convection, consistent with the cloud structure observed in Fig. 7a: convection over La Réunion is forced by the residuals of tropical cyclone Fami that has landed over Madagascar. The 25 June (Fig. 8b1–b3), the mean reflectivity increases from 15:00 to 16:30 UTC and between 17:15 and 19:15 UTC, with some strong peaks of 46 dBZ. On that day, such strong reflectivity is not observed above 3 km height. Strong reflectivities are associated to downward motion (w around $-5\,m\,s^{-1}$, Fig. 8b2). The wind is from the south east until 16:00 UTC and from the east in the lower levels. Above 1000 m, it is from north east. The intensity of the wind (Fig. 8b3) is less than $12\,m\,s^{-1}$ and can reach $18\,m\,s^{-1}$ for some short period of time.

AMTD
6, 3249–3277, 2013

At 4.5 km, a trade wind inversion is observed, characterizing a change in horizontal wind direction and by vanishing vertical velocities. Such a case corresponds to the end of the passage of a cold front from the mid-latitudes (Fig. 7b).

The 19 August (Fig. 8c1–c3), reflectivities are less intense than for the other case studies, since they attain only 31 dBZ during a short period of time. Moreover, strong reflectivities only appear below 2 km, which suggests that rain does not occur above this altitude. Again such strong reflectivities are correlated to weak vertical velocity (less than $-4\,\mathrm{m\,s^{-1}}$) (Fig. 8c2). The wind is south easterly (Fig. 8c3), more intense ($18\,\mathrm{m\,s^{-1}}$) than the others cases in the lower levels. The trade winds inversion may be observed around 4 km. The strong horizontal winds in the low levels are explained by the existence of a winter depression, South of La Réunion (Fig. 7c). The satellite image also suggests that clouds are restricted to the low-levels.

3.2.2 Parameters of the gamma function

Figure 9 (1–3) displays time-height sections of the three parameters describing the shape of the DSD that is Λ (LA on the figure), μ and N_o for the three cases analysed. At a first glance, one can notice that roughly strong reflectivities are associated to low Λ, μ and N_o values and that these gamma DSD parameters are well correlated (more than 0.72) between them (a4 to c4). On 2 February, the value of N_o and μ are lower than the other days since reflectivity is higher. The slopes are nearly the same for the 25 June and 19 August, but it is less for the 2 February.

As explained previously the methodology relies on an empirical quadratic μ–Λ relationship. Equation (4) is one of the equations listed by Chu and Su (2008) but in which the coefficients were slightly modified. According to Chandrasekhar and Bringi (1987), because N_o involves units that depend on μ, there is a strong correlation between μ and N_o in the three cases (not show here). Ulbrich (1983) show that the resulting fit between $N_o$and μ is

$$N_o = 60\,000\exp(3.2\mu)\mathrm{m^{-3}\,cm^{-1-\mu}} \quad (10)$$

AMTD
6, 3249–3277, 2013

with a range from $10^{5.5}\exp(2.8\mu)$ to $10^{4.2}\exp(3.57\mu)\,\mathrm{m}^{-3}\,\mathrm{cm}^{-1-\mu}$. Illingworth and Blackman (2002) reported that such relationship arises because of the particular form of the gamma function $N(D)$.

3.2.3 Rain rate

Figure 10 presents the time-height sections of the precipitation rate R (1), and a comparison between the rain rate obtained by the radar and obtained by the raingauge (2). Strong reflectivity (Fig. 8) is associated to strong precipitation. So, strong precipitation rate are well correlated to weak parameters Λ, μ and N_o.

Comparisons between the rain rate obtained by the radar and by the raingauge clearly show that the radar underestimates the precipitation on the 2 February. The wind profiles observed on that day (Fig. 8a3) reveal strong wind shear in the lower altitudes. This is consitent with the difference rain rate between 800 m and the ground (Fig. 5). The best agreement is observed on the 19 August when the rain rate is weak.

Figure 10 (a3-b3-c3) also presents a plot of the rain rate deduced from the actual gamma methodology versus the rain rate obtained using an exponential distribution ($\mu = 0$, Marshall–Palmer law). The least square fit of the data shows a good agreement between both estimates (around 1.03 for the 2 February: $R_{\mathrm{gamma}} = 1.03\, R_{\mathrm{marshall}}$) with strong correlation coefficient (more than 0.99 for the three cases). On the 19 of August, the agreement of the rain rate obtained by the two methods is weaker (i.e only 0.86), which could be due to the lower rain rates and stronger Λ, N_o and μ parameters. In such a case, the gamma function should be used (Wilks, 1995). Although there is some certain data dispersion around the fit for the 2 February and for the 25 June, an exponential DSD (good correlation between R from gamma distribution and R from exponential distribution) is acceptable and accurate enough for obtaining rain integrated quantities from radar data. It is simpler to use than the gamma distribution since it does not involve the selection of a quadratic form between μ and Λ. This conclusion was also reached by Smith (2003).

AMTD
6, 3249–3277, 2013

As a summary, radar UHF data reproduces well rain rates and rainfall velocities, which allows to use its data to determine kinetic fluxes.

3.2.4 Kinetic energy fluxes

The panel displayed in Fig. 11a–c illustrates some results on the retrieval by the profiler of parameters related to soil erosion. The mean vertical profile of VKEF and HKEF, the rain vertical and horizontal kinetic energy flux respectively, synthesizes the vertical variation of these parameters presented in the time-height sections. Compared to HKEF, VKEF shows on average a weak evolution with height for the three cases which can be related to the vertical constancy of the rain characteristics. On 19 August, HKEF and VKEF vanishes with height above 2.5 km following rain rate that we can notice in Fig. 8b3. For this case study the figure shows that the contribution on the erosion process by the rain vertical kinetic energy can be considered negligible compared to the horizontal one up to an altitude of 2.5 km. Figure 11 (a3-b3-c3) also displays a linear least square fit between the reflectivity factor Z and VKEF. The relationship obtained with a correlation coefficient higher than 0.99 is VKEF = $\alpha Z^{0.9}$ with units in mW m^{-2} and mm^6 m^{-3}. α is slighly different for each case study; it is 0.024 on 19 August, 0.0315 on 25 June and 0.0257 on the 2 February.

4 Conclusions

One year (May 2009–April 2010) of UHF radar data has been analyzed in La Réunion. The properties of rainfall during the moist and dry seasons are observed. The moist season corresponds to the maximum of mean rainfall at all levels. During the dry season, the highest rain rates are around 1.2 km and rain is limited by the trade wind inversion. The passage of fronts may carry more rain but vertical extension is limited by the trade wind inversion. Three cases from each season have been analyzed showing that the three gamma DSD parameters are weaker for the stronger rain rates. The

AMTD
6, 3249–3277, 2013

rain rate obtain by gamma function is nearly the same than those obtained by the Marshall Palmer equation for the moist-season case (the slope of the least square fit of the data is 1.03). For each case analyzed, the horizontal kinetic fluxes are always higher than the vertical kinetic energy fluxes.

The next step will be to analyze the horizontal and vertical kinetic fluxes for the different season as it was done for the rain rate. We have restricted the analysis here to the rain kinetic energy but an other important parameter that plays a role in the rain erosivity is the orientation of the drop fall angle with respect to the slope terrain direction. The drop fall angle is easy to calculate with the profiler data since it is the vectorial addition of the intrinsic drop fallspeed with the horizontal wind.

It would be also interesting to analyze the different winds in the vertical profile of the radar and near the mountain using a Large Eddy Simulation model for two case studies (strong winds, weak winds).

Acknowledgements. We acknowledge Meteo France for providing the mean precipitation in la Réunion and rain rate time series. We want also to acknowledge Cheikh Dione and Christelle Barthe for their great help. To finish, we acknowledge also Hélène Ferré, Yann Courcoux, Serge Prieur and Franck Gabarrot for radar data collection and management.

The publication of this article is financed by CNRS-INSU.

AMTD
6, 3249–3277, 2013

References

Atlas, D., Srivastava, R. C., and Sekkon, R. S.: Doppler radar characteristics of precipitation at vertical incidence, Rev. Geophys. Space GE, 2, 1–35, 1973.

Baldy, S., Ancellet, G., Bessafi, M., Badr, A., and Lan Sun Luk, D.: Field observations of the vertical distribution of tropospheric ozone at the island of Réunion (southern tropics), J. Geophys. Res., 101, 23835–23849, doi:10.1029/95JD02929, 1996.

Brandes, E. A., Zhang, G., and Vivekanandan, J.: Comparison of polarimetric radar drop size distribution retrieval algorithms, J. Atmos. Ocean. Tech., 21, 584–598, 2004.

Campistron, B. and Réchou, A.: Rain kinetic energy measurement with a UHF wind, 13th International Workshop on Technical and Scientific Aspects of MST Radar, 19–23 March 2012, Kühlungsborn, 2012.

Chandrasekar, V. and Bringi, V. N.: Simulation of radar reflectivity and surface measurements of rainfall, J. Atmos. Ocean. Tech., 4, 464–478, 1987.

Chen, C.-S. and Chen, Y.-L.: The rainfall characteristics of Taiwan, Mon. Weather Rev., 131, 1323–1341, 2003.

Chen, T.-C., Yen, M.-C., Hsieh, J.-C., and Arritt, R. W.: Diurnal and seasonal variations of the rainfall measured by the automatic rainfall and meteorological telemetry system in Taiwan, B. Am. Meteorol. Soc., 80, 2299–2312, 1999.

Chu, Y.-H. and Su, C.-L.: An investigation of the slope-shape relation for gamma raindrop size distribution, J. Appl. Meteorol. Clim., 47, 2531–2544, 2008.

Cifelli, R., Williams, C. R., Rajopadhyaya, D. K., Avery, S. K., Gage, K. S., and May, P. T.: Drop-size distribution characteristics in tropical mesoscale convective systems, J. Appl. Meteorol., 39, 760–777, 2000.

Courtillot, V., Besse, J., Vandamme, D., Montigny, R., Jaeger, J.-J., and Capetta, H.: Deccan flood basalts at the cretaceous/tertiary boundary?, Earth Planet. Sc. Lett., 80, 361–374, 1986.

Feingold, G. and Levin, Z.: The lognormal size distribution of raindrops: application to differential reflectivity measurements of rainfall (ZDR), J. Atmos. Ocean. Tech., 4, 377–382, 1987.

Foote, N. H. and du Toit, P. S.: Terminal velocity of raindrop aloft, J. Appl. Meteorol., 8, 585–591, 1969.

Gossard, E.: Measuring drop-size distributions in clouds with a clear-air-sensing Doppler radar, J. Atmos. Ocean. Tech., 5, 640–649, 1988.

AMTD
6, 3249–3277, 2013

Gossard, E., Strauch, R. G., and Rogers, R. R.: Evolution of drop-size distribution in liquid precipitation observed by ground-based Doppler radar, J. Atmos. Ocean. Tech., 7, 815–828, 1990.

Hastenrath, S.: Climate Dynamics of the Tropics, retrieved on 29 February 2009, Springer, 244 pp., 1991.

Illingworth, A. J. and Blackman, T. M.: The need to represent raindrop size spectra as normalized gamma distributions for the interpretation of polarization radar observations, J. Appl. Meteorol., 41, 286–297, 2002.

Johnson, R. H. and Bresch, J. F.: Diagnosed characteristics of precipitation systems over Taiwan during the May–June 1987 TAME X, Mon. Weather Rev., 119, 2540–2557, 1991.

Kozu, T. and Nakamura, K.: Rainfall parameter estimation from dual-radar measurements combining reflectivity profile and path-integrated attenuation, J. Atmos. Ocean. Tech., 8, 259–270, 1991.

Maguire, W. B. and Avery, S. K.: Retrieval of raindrop size distributions using two Doppler wind profilers: model sensitivity testing, J. Appl. Meteorol., 33, 1623–1635, 1994.

Marshall, J. S. and Palmer, W. M.: The distribution of raindrops with size, J. Meteorol., 5, 165–166, 1948.

Murata, F., Yamanaka, M., Fujiwara, M., Ogino, S.-Y., Hashigushi, H., Fukao, S., Kudsy, M., Sribimawati, T., Harijono, S. W. B., and Kelana, E.: Relationship between wind and precipitation observed with a UHF radar, GPS rawindsondes and surface meteorological instruments at Kototabang, West Sumatera during September–October 1998, J. Meteorol. Soc. Jpn., 80, 347–360, 2002.

Quetelard, H., Bessemoulin, P., Cerveny, R. S., Peterson, T. C., Burton, A., and Boodhoo, Y.: World record rainfalls (72-hour and four-day accumulations) at Cratère Commerson, Réunion Island, during the passage of Tropical Cyclone Gamede, B. Am. Meteorol. Soc., 90, 603–608, 2009.

Rajopadhyaya, D. K., May, P. T., and Vincent, R. A.: A general approach to the retrieval of rain drop size distributions from wind profiler Doppler spectra: modelling results, J. Atmos. Ocean. Tech., 10, 710–717, 1993.

Rajopadhyaya, D. K., Avery, S. K., May, P. T., and Cifelli, R. C.: Comparison of precipitation estimation using single- and dual-frequency wind profilers: simulations and experimental results, J. Atmos. Ocean. Tech., 16, 165–173, 1999.

AMTD
6, 3249–3277, 2013

Robert, R.: Climat et hydrologie à la Réunion: etude typologique et régionale des pluies et de l'écoulement, Thèse, Univ. de Montpellier, 438 pp., 1986.
Sanderson, M. (Ed.): Prevailing trade-winds, in: Weather and Climate in Hawaii, University of Hawaii Press, 126 pp., 1993.
Schafer, R., Avery, S., May, P., Rajopadhyaya, D., and Williams, C.: Estimation of rainfall drop size distributions from dual-frequency wind profiler spectra using deconvolution and a non-linear least squares fitting technique, J. Atmos. Ocean. Tech., 19, 864–874, 2002.
Schroeder, T. A.: Climate controls, Prevailing Trade Winds: Weather and Climate in Hawaii, edited by: Sanderson, M., University of Hawaii Press, 12–36, 1993.
Smith, R. B.: A linear upslope-time-delay model for orographic precipitation, J. Hydrol., 282, 2–9, 2003.
Su, C.-L. and Chu, Y.-H.: Analysis of terminal velocity and VHF backscatter of precipitation particles using Chung–Li VHF radar combined with a ground-based disdrometer, Terr. Atmos. Ocean. Sci., 18, 97–116, 2007.
Taupin, F. G., Bessafi, M., Baldy, S., and Bremaud, P. J.: Tropospheric ozone above the south-western Indian Ocean is strongly linked to dynamical conditions prevailing in the tropics, J. Geophys. Res., 104, 8057–8066, doi:10.1029/98JD02456, 1999.
Ulbrich, C. W.: Natural variations in the analytical form of theraindrop size distribution, J. Clim. Appl. Meteorol., 22, 1764–1775, 1983.
Ulbrich, C. W. and Atlas, D.: Rainfall microphysics and radar properties: analysis methods for drop size spectra, J. Appl. Meteorol., 37, 912–923, 1998.
Wakasugi, K., Mizutani, A., Matsuo, M., Fukao, S., and Kato, S.: A direct method for deriving drop-size distributiona and vertical air velocities from VHF Doppler radar spectra, J. Atmos. Ocean. Tech., 3, 623–629, 1986.
Wilks, D. S.: Statistical Methods in the Atmospheric Sciences, Academic Press, 467 pp., 1995.
Williams, C. R.: Simultaneous ambient air motion and raindrop size distributions retrieved from UHF vertical incident profiler observations, Radio Sci., 37, 1024, doi:10.1029/2000RS002603, 2002.
Zhang, G., Vivekanandan, J., Brandes, E., Meneghini, R., and Kozu, T.: The shape-slope relation in observed gamma raindrop size distribution: statistical error or useful information?, J. Atmos. Ocean. Tech., 20, 1106–1119, 2003.

AMTD
6, 3249–3277, 2013

Fig. 1. La Réunion Island in the Indian Ocean. The UHF wind profiler is located at Saint-Denis Airport (20°53′33″ S, 55°31′44″ E).

AMTD
6, 3249–3277, 2013

One-year analysis of rain and rain erosivity in a tropical volcanic island

A. Réchou et al.

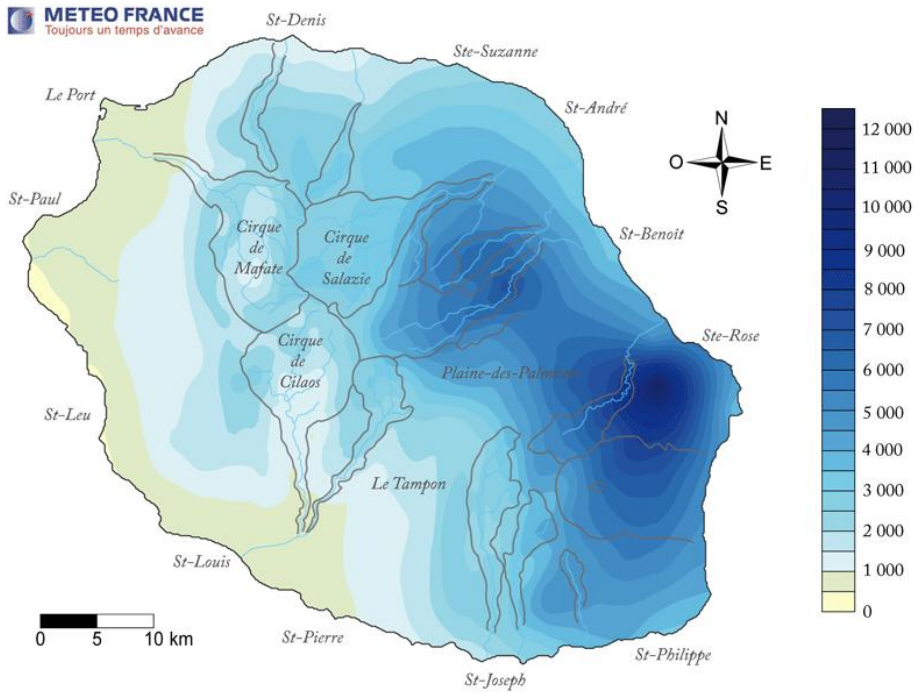

Fig. 2. Annual mean precipitation (mm) obtain from 1981 to 2010.

AMTD
6, 3249–3277, 2013

Fig. 3. Antenna of the UHF wind profiler.

AMTD
6, 3249–3277, 2013

One-year analysis of rain and rain erosivity in a tropical volcanic island

A. Réchou et al.

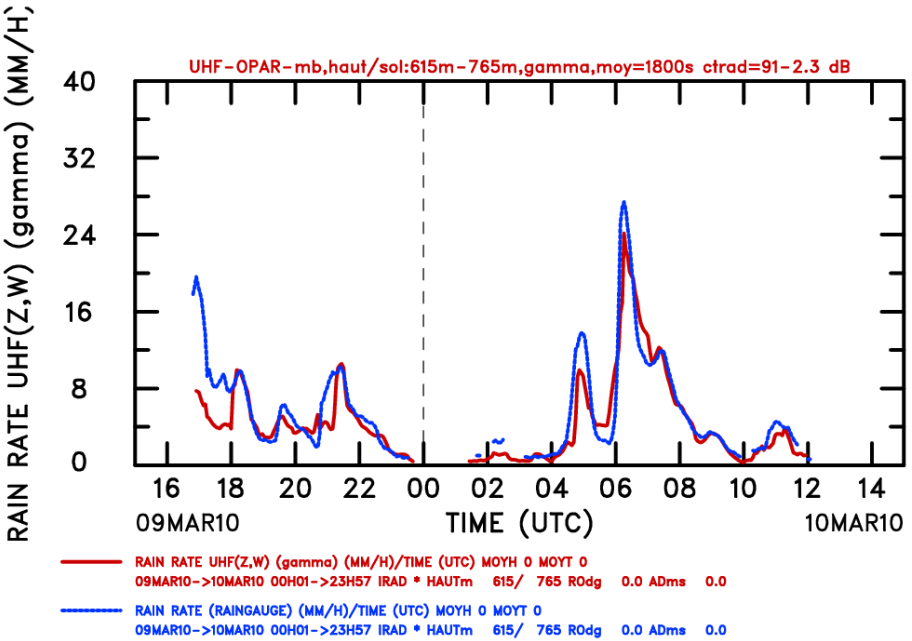

Fig. 4. Time series of the rain rate deduced from the UHF profiler data during the considered period between 615 and 765 m and superposed the rain rate given by a raingauge at sea level.

AMTD
6, 3249–3277, 2013

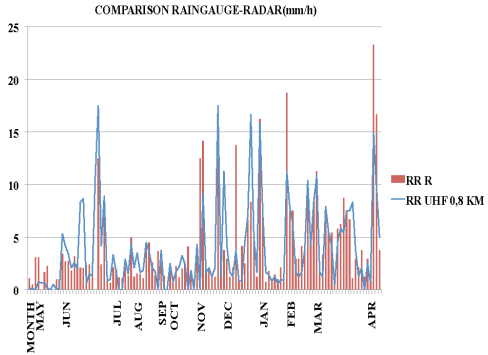

a)

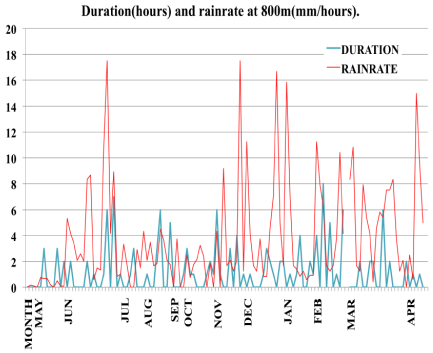

b)

Fig. 5. (a) Comparison between rainrate from the radar data (800 m) and from the raingauge located beside the radar and **(b)** comparison between rainrate from the radar data (800 m) and duration of the rain (800 m) for the period between April 2009 to April 2010.

AMTD
6, 3249–3277, 2013

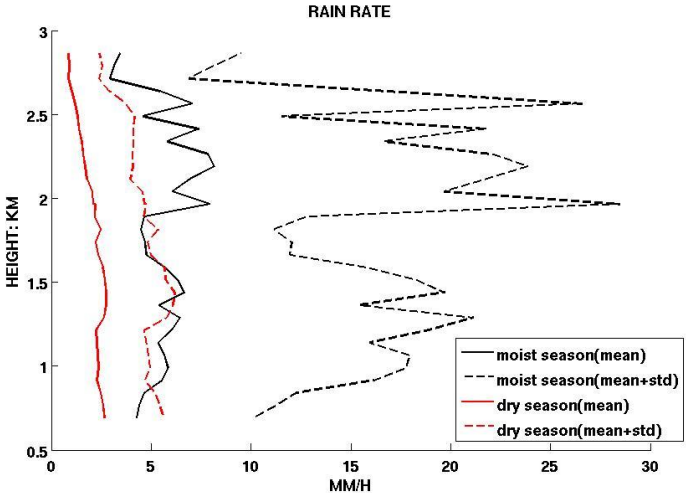

Fig. 6. Profil of mean rain rate (-) and standard deviation precipitation (–) observed during the rain season (November 2009 to March 2010) in dark and during the dry season (April to October 2009 and April 2010) in red.

AMTD
6, 3249–3277, 2013

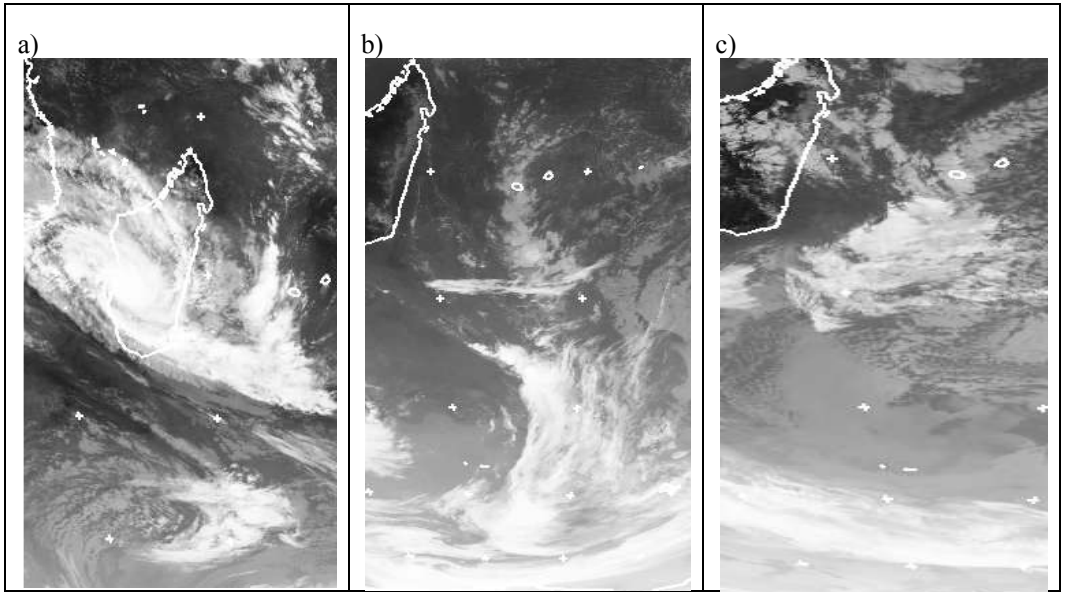

Fig. 7. Thermal infrared (10.5–12.5 µm) Meteosat VISSR (IODC) 057.0E Quicklooks at 12:00 UTC for **(a)** the second of February, **(b)** the 25 June and **(c)** the 19 August. Such image are provided by Meteosat.

AMTD
6, 3249–3277, 2013

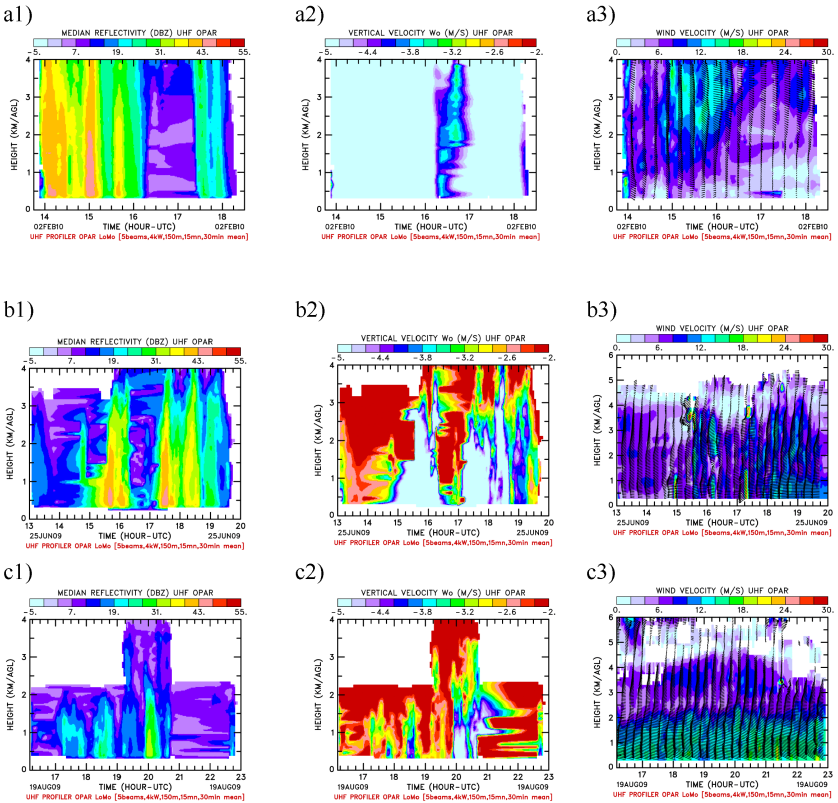

Fig. 8. Time-height sections for the rain air of reflectivity factor $Z(1)$, of vertical velocity (W) deduced from the 5 beam(2) and intensity and direction of horizontal wind $V(3)$ for **(a)** the 2 February 2010 (lower mode), **(b)** the 25 June 2009 and **(c)** the 19 August 2009 (upper mode). Note that in **(c3)** there are more data, since all the particules was taking into account (to see trade wind inversion), for **(a3)** and **(b3)** selection of rain have be done.

AMTD
6, 3249–3277, 2013

One-year analysis of rain and rain erosivity in a tropical volcanic island

A. Réchou et al.

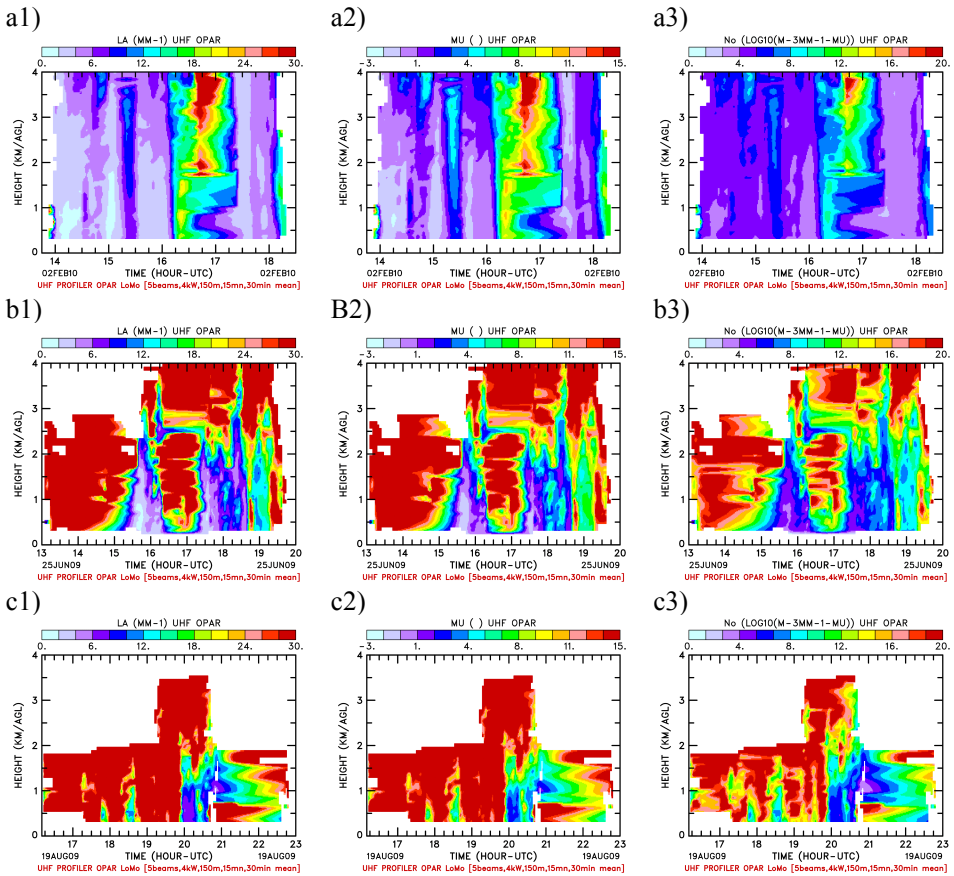

Fig. 9. Time-height sections of $\Lambda(1)$, $\mu(2)$ and $N_o(3)$ the three shape parameters of the rain drop size distribution deduced from profiler data for **(a)** the 2 February 2010, **(b)** the 25 June 2009 and **(c)** the 19 August 2009. An average over 30 min is applied.

AMTD
6, 3249–3277, 2013

One-year analysis of rain and rain erosivity in a tropical volcanic island

A. Réchou et al.

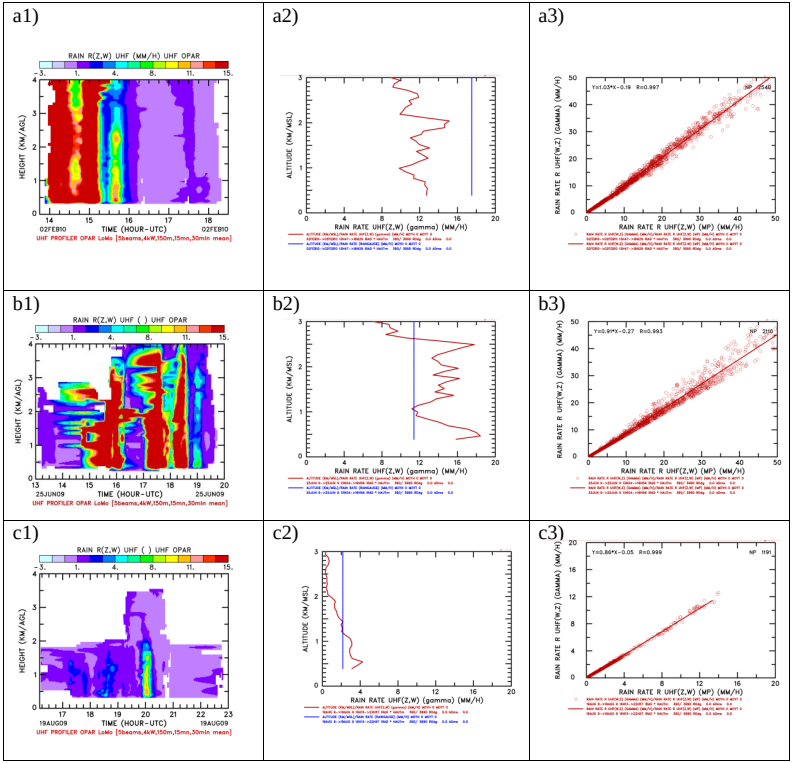

Fig. 10. Time-height sections of R the precipitation rate (1), mean profile of rain rate obtain during the same period and associate rain rate given by a raingauge at sea level (2) and rain rate computed with Gamma DSD versus rain rate computed with exponential DSD ($m = 0$, MP) with linear fit (3) for **(a)** the 2 February 2010, **(b)** the 25 June 2009 and **(c)** the 19 August 2009. KM/AGL (Above Ground Level) and KM/MSL (Mean Sea Level) are considered to be the same in our case.

AMTD
6, 3249–3277, 2013

One-year analysis of rain and rain erosivity in a tropical volcanic island

A. Réchou et al.

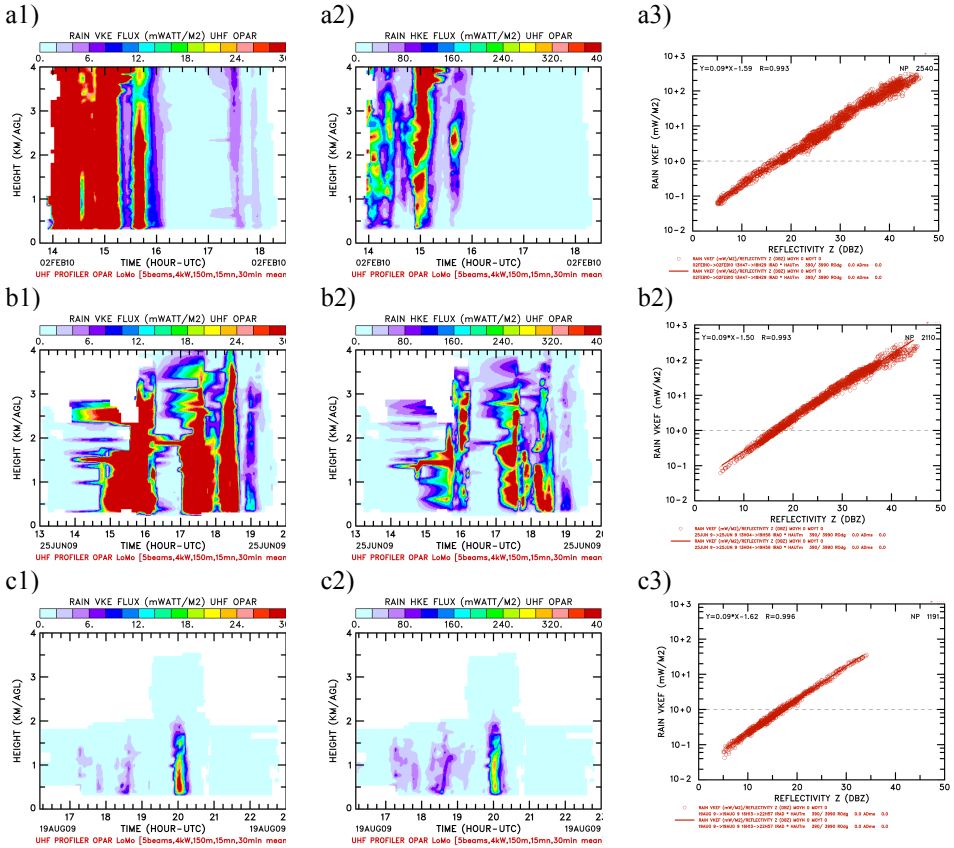

Fig. 11. Time-height sections of the rain vertical (1) and horizontal (2) kinetic energy flux (VKEF and HKEF) and plot of VKEF against reflectivity factor Z (3) for the same data with a linear fit for **(a)** the 2 February 2010, **(b)** the 25 June 2009 and **(c)** the 19 August 2009. A 30 min average is used.

AMTD
6, 3249–3277, 2013

One-year analysis of rain and rain erosivity in a tropical volcanic island

A. Réchou et al.